Exact and Efficient Crosstalk Estimation

Martin Kuhlmann, Member, IEEE and Sachin S. Sapatnekar, Member, IEEE

Abstract

With the reducing distances between wires in deep sub-micron technologies, coupling capacitances are becoming significant as their magnitude becomes comparable to the area capacitance and fringing capacitance of a wire. This causes an increasing susceptibility to failure due to inadvertent noise, and leads to a requirement for accurate noise estimation. An incorrect estimation of the noise could lead either to circuit malfunction in case of under-estimation, or to wasted design resources due to overestimation. This paper presents a new time-efficient method for the precise estimation of crosstalk noise. While existing fast noise estimation metrics may overestimate the coupling noise by several orders of magnitude, the proposed metric computes the coupling noise with a good accuracy as compared to SPICE. [1]

1 Introduction

In the past, timing and power analysis have been the critical criteria to be optimized in the design process. With the use of deep sub-micron technologies, shrinking geometries have led to a reduction in the self-capacitance of wires while increasing coupling capacitances as wires are brought closer together. In conjunction with increases in operating frequencies, noise analysis and avoidance is becoming as critical a factor in circuit design as timing or power. For present day processes, the coupling capacitance can be as high as the sum of the area capacitance and the fringing capacitance of a wire, and trends indicate that the role of coupling capacitances will be even more dominant in the future as feature sizes shrink [1, 2].

[1]This work was supported in part by the Defense Advanced Research Projects Agency under contract number DA/DABT63-96-C-0050, by the Semiconductor Research Corporation under contract 98-DJ-609 and by the National Science Foundation under award CCR-9800992.

Martin Kuhlmann was with the Department of Electrical and Computer Engineering, University of Minnesota, Minneapolis MN 55455, USA. He is now with Broadcom Corporation, Irvine, CA 92619, USA.

Sachin S. Sapatnekar is with the Department of Electrical and Computer Engineering, University of Minnesota, Minneapolis MN 55455, USA.

One of the important effects of coupling capacitances is that they may induce unwanted voltage spikes in neighboring nets. A net on which a switching event occurs is termed an *aggressor* and the net on which it produces a noise spike is referred to as a *victim*. Typically, an aggressor net is physically adjacent to a victim net and they may be modeled as being connected by a distributed coupling capacitance. Hence, a switching event in the aggressor net while the victim net is silent can result in the injection of a $C\frac{\mathrm{d}v}{\mathrm{d}t}$ current into the victim net, causing an electrical spike. In static CMOS circuits, in time, as the aggressor net completes its transition, this electrical spike dies down to zero. However, a large coupling capacitance relative to the self-capacitance of the wire can cause a large inadvertent spike on the victim that may cause a spurious switching event, potentially leading to an unintended state being latched and thereby changing the functionality of the circuit.

Various transient analysis techniques can be used to estimate noise. Circuit or timing simulation techniques, such as SPICE [3], may be used, but these are computationally expensive and are not conducive to use on large systems, particularly when fast noise evaluations for noise optimization purposes are required. When the system is modeled as a linear circuit, linear model order reductions such as [4, 5, 6] may be used, and these have been incorporated in a noise evaluation system [7, 8]. These model order reduction techniques help in reducing the computational cost, but in several cases, the cost is still unacceptably high for an optimization system that would use a noise metric to select the circuit parameters for noise-free behavior. Using modern moment matching methods, it may still require more than a day to compute the noise in a modern microprocessor [9]. An example of such a situation is in designing a physical design system where optimizations such as buffer insertion [10], spacing [11] or routing criteria are to be introduced [12, 13, 14]; such systems must, of necessity, use much simpler noise metrics. Most existing physical design systems for noise optimization use extremely simple noise models such as one where the noise is computed as being proportional to the overlap between wires [12, 13, 14]. While this is not an unreasonable first-order model, it fails to capture deeper intricacies such as the effects of the slope of the aggressor transient waveform, the effects of the ratio of the self-capacitance to the coupling capacitance, etc. As these simple formulae do not have a concrete electrical and circuit theoretic formulation, they are liable to be inaccurate.

A fast metric for coupled noise estimation based on model-order reduction techniques was recently presented in [9]. We will describe this metric in detail in Section 3, and it forms the foundation for this work. However, while it is an excellent first effort, its limitations lie in the fact that it computes only an upper bound on the circuit noise, a value that is overly pessimistic. While we will explicitly list and quantify its other weaknesses later in this paper, it suffices to observe here that its accuracy is limited to short wires and relatively slow slew rates of more than 100ps. In the near future, when clock frequencies of 1-2 GHz will be common, much faster slew rates are expected and due to resistive shielding slew rates of 20ps to 100ps can be obtained at the driver output. Hence, the upper bound is too pessimistic and is liable to predict noise spikes that exceed the supply voltage, which is impossible in a pure RC circuit. This motivates the need for a more accurate metric for noise analysis to address these problems. While in [15] a piecewise linear input and a first order model of the noise is used, we now utilize a third order model of the noise and an exponential voltage source. This leads to much more accurate results including the exact modeling of the noise tail.

This paper presents an improved metric for a more precise estimation of crosstalk noise. Its computational complexity is comparable to the Devgan metric and its derivation is, indeed, inspired by the techniques used in that metric. Our experimental results show the improved accuracy of the method.

The paper is organized as follows. Section 2 presents the basics of crosstalk estimation, followed by a brief presentation of Devgan's metric in Section 3. Section 4 and 5 present the new efficient noise estimation method for pure capacitive coupled nets and for capacitive and inductive coupled nets. Procedures for efficient computation and an analysis of the computational complexity are provided in Section 6. Experimental results are listed in Section 7 and a set of concluding remarks round up the paper in Section 8.

2 Basics of Crosstalk Estimation

The work in [9] introduced a method for computing an estimate of the coupling noise between wires using the final value theorem [16]. The method was elegant in its simplicity in that it permitted the noise estimate to be calculated in a similar manner to the Elmore delay [17]. This

led to its adoption for use in physical design in [10, 11], using an extension of Elmore delay optimization methods for this purpose.

The method proposed in this work begins with the same equations as [9], but performs a different analysis for noise estimation. While Devgan's metric is guaranteed to be an upper bound on the noise, we will show that it may be too pessimistic, and that it may be wiser not to employ the final value theorem to develop a metric based on this approach for systems with fast switching transitions at gate outputs. To illustrate this, we show the difference between the two methods in Figure 1. In [9], the aggressor net is assumed to be excited by a forcing function that is similar to a step function, but with a nonzero transition time and a finite slope. This slope leads to a noise spike in the victim net of the type shown by graph 2 in the figure. However, to ease the computation, it was assumed in [9] that the increasing ramp is infinite, leading to the response shown by graph 1 in the figure. This is easily proven to be an upper bound on the noise shown in graph 2.

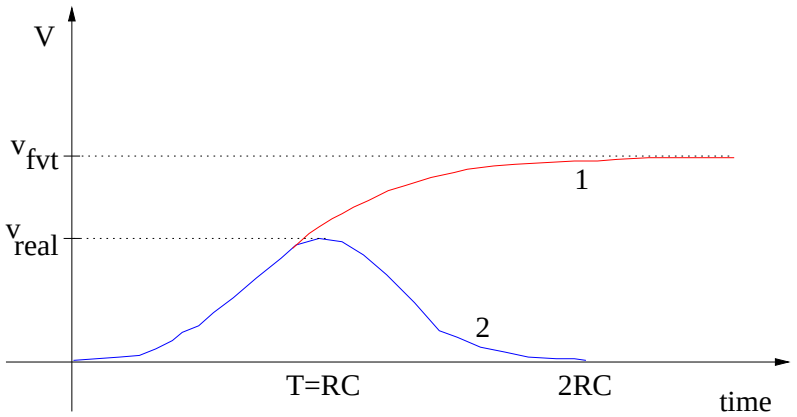

Figure 1. Different model for analyzing the noise. 1 shows final value theorem method, 2 shows real noise signal used for the proposed method

However, this upper bound is not necessarily tight, and we will show instances in our experimental results where the bound leads to meaningless results since the obtained value is larger than V_{dd}. As shown in Figure 1, the noise reaches its maximum value at some time after the aggressor net switches, after which it again decreases towards zero. Nevertheless, it is certainly true that in order to approximate the noise, the slew rate of the aggressor plays an important role since it influences the $C\frac{dv}{dt}$ current injected into the victim through the coupling capacitance.

This current causes the voltage to drop along the wire resistance of the victim net. Assuming the victim net to be at zero potential initially, the voltage at a node on the victim net first increases due to this injection. As the transient on the aggressor net settles, the magnitude of the injected current reduces, and the noise on the victim net dies down to zero.

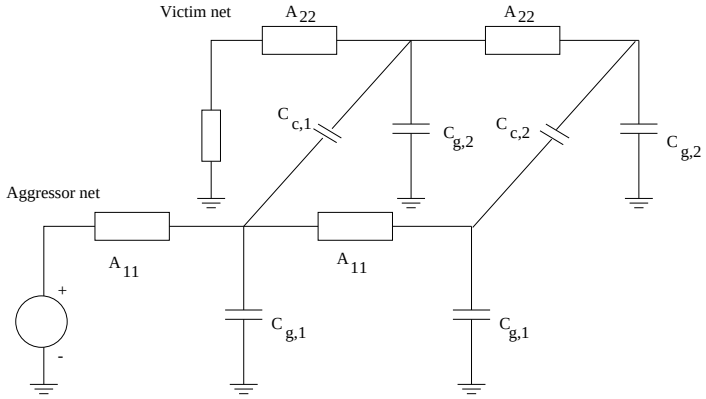

Figure 2. Circuit schematic with aggressor and victim net for coupled noise. For the sake of simplicity, only two of the n distributed RC elements have been shown.

We will now soon reproduce the essentials of Devgan's approach to formulating the problem, and we will utilize the same basic notation to express our solution to the problem. The basic set of equations for a circuit of the type shown in Figure 2, with net 1 being the aggressor and net 2 being the victim net, initially at ground potential, can be written as follows:

$$\begin{bmatrix} C_1 & -C_c^T \\ -C_c & C_2 \end{bmatrix} \begin{bmatrix} \dot{v_1} \\ \dot{v_2} \end{bmatrix} = \begin{bmatrix} -A_{11} & 0 \\ 0 & -A_{22} \end{bmatrix} \begin{bmatrix} v_1 \\ v_2 \end{bmatrix} + \begin{bmatrix} B_1 \\ 0 \end{bmatrix} v_s, \tag{1}$$

where v_1 is a vector of node voltages in the aggressor net, v_2 is a vector of node voltages in the victim net, and v_s is the input to the aggressor net. In (1), the zeros in the conductance matrix indicate the fact that there is no resistive path between net 1 and net 2. The zero on the right hand side is due to the fact that the excitation is applied only to net 1 and net 2 is connected to ground. Although this example illustrates a two-segment net, the equations for nets with larger numbers of segments can be written similarly: the capacitances and the A values, which are scalars here, will be replaced by capacitance matrices, and vectors will be used to represent the voltages and the input excitations. This matrix system can be rewritten in the Laplace domain

as

$$\begin{aligned} sC_1V_1 - sC_c^TV_2 &= -A_{11}V_1 + B_1V_s, \\ sC_cV_1 - sC_2V_2 &= A_{22}V_2. \end{aligned} \tag{2}$$

Note that the diagonal entries of capacitance matrices C_1 and C_2 correspond to the sum of ground and coupling capacitances, while diagonal entries of the matrix C_c have a positive value.

3 Description of Devgan's Metric

Using Equation (2), Devgan computes the transfer function

$$\begin{aligned} H(s) &= \frac{V_2(s)}{V_s(s)} \\ &= -\left[-\left(sC_2 + A_{22}\right) + sC_c\left(sC_1 + A_{11}\right)^{-1} sC_c^T\right]^{-1} \cdot \\ &\qquad sC_c\left(sC_1 + A_{11}\right)^{-1} B_1 \end{aligned} \tag{3}$$

Applying an input voltage, V_s, to the aggressor net in the form of a finite ramp leads to a solution to the circuit. However, since this could lead to a messy solution procedure, Devgan applies an input of the form k/s^2. This corresponds to an infinite ramp of slope k, the response to which, as observed earlier, is a monotone increasing waveform on the victim whose final value provides an upper bound on the noise. Applying the final value theorem leads to the result

$$V_{2,max} = -A_{22}^{-1}C_cA_{11}^{-1}B_1k \tag{4}$$

To simplify the process of calculating this, a circuit interpretation was provided. Equation (4) can be rewritten as

$$V_{2,max} = -A_{22}^{-1}C_c\dot{V}_{1,ss}, \tag{5}$$

where

$$\dot{V}_{1,ss} = A_{11}^{-1}B_1k. \tag{6}$$

The circuit interpretation of this implies that (6) may be solved by applying an excitation of B_1k to the aggressor net 1 while open-circuiting all capacitances connected to it. This implies that for an RC aggressor line with no path to ground, the value of $\dot{V}_{1,ss} = k$ at all nodes. Considering the

circuit interpretation of $C_c\dot{V}_{1,ss}$ in Equation (5), each coupling capacitance can be replaced by a current source of value k times the coupling capacitance at the node; any capacitances to ground are removed. Let us represent this vector of current sources be I_c. Then solving (5) amounts to solving

$$V_{2,max} = -A_{22}^{-1} I_c. \tag{7}$$

Thus, the value of $V_{2,max}$ can be obtained by solving net 2 with the above transformation on all capacitances. This may be carried out by means of a tree traversal.

3.1 Limitations of this Metric

The metric described above has several limitations:

- The noise voltage in the victim net is proportional to the slope of the transient of the input voltage ramp. In case of fast slew rates, the noise of the victim increases in an unbounded manner. In the extreme situation where the input is a step function, the noise in the victim net goes to ∞. This is clearly impossible since the supply voltage limits the maximum noise that can be induced.

- The magnitude of the induced noise has no dependence whatsoever on the capacitances to ground of either the aggressor or the victim. This is clearly incorrect, since a coupling capacitance that is negligible in comparison with the capacitance to ground would lead to a negligible crosstalk value. Moreover, there is no dependence on the resistances in the aggressor net, implying that the length of the aggressor net is irrelevant to the value of the noise spike.

In Tables 1 and 2, we support the two arguments above by explicit verification. The results in the two tables show the noise spike in Volts using parameters for a 0.25μm technology and for a 0.18μm technology, respectively. For the length of the victim net, four different lengths, varying from 0.5mm to 5mm, have been assumed. Additionally, four different slew rates have been used. The "x" in the Tables 1 and 2 represents the independence of the noise to the length of the aggressor net. It is seen from the tables that the predicted noise spike greatly exceeds the V_{dd} value. According to our HSPICE simulations, the magnitude of the crosstalk spike on a victim

Table 1. Noise simulation results in Volt of Devgan's metric using a 0.25μm CMOS technology and V_{dd}=2.5V. The wires have been spaced at twice the minimum distance leading to a resistance, a ground and coupling capacitance per mm of 146 Ω, 70.8 fF and 71 fF, respectively.

wire length, aggressor-victim	20ps	50ps	100ps	250ps
x-5mm	64.9V	25.77V	19.47V	7.74
x-2.5mm	16.54V	6.56V	4.96V	1.98
x-1mm	2.8V	1.11V	0.84V	0.334
x-0.5mm	0.76V	0.3V	0.22V	0.091

Table 2. Noise simulation results in Volt of Devgan's metric using a 0.18μm CMOS technology and V_{dd}=1.8V. The wires have been spaced at twice the minimum distance leading to a resistance, a ground and coupling capacitance per mm of 250 Ω, 51.4 fF and 58.3 fF, respectively.

wires	20ps	50ps	100ps	250ps
x-5mm	50.27V	19.96V	15.08V	6V
x-2.5mm	12.82V	5.08V	3.84V	1.53V
x-1mm	2.16V	0.86V	0.65V	0.25V
x-0.5mm	0.59V	0.23V	0.17V	0.07V

net of constant length can vary by as much as 64 % with variations in the length of the aggressor. This has been obtained by assuming a victim length of 0.5mm and a variable aggressor length either 1mm and 5mm, respectively. Due to the larger capacitive load on the aggressor, the slew of the aggressor is degraded and induces less current into the victim. In our simulations, we placed the victim and aggressor driver always adjacent to eachother. However, this is no limitation of the new metric.

4 A New Metric for Precise Crosstalk Estimation

We will persist with the notation introduced above, as far as possible, and model the input voltage as an exponential function according to

$$v_s(t) = V_{dd}(1 - e^{-t/p})u(t) \tag{8}$$

where p corresponds to the time constant of the driver of the aggressor. This time constant can be computed by using effective wire capacitance C_{eff} and the driver impedance.

For an exponential input, we may expand $V_1(s)$ using the series:

$$V_1(s) = v_{10}s^{-1} + v_{11} + v_{12}s + v_{13}s^2 + ... \tag{9}$$

Similarly, the voltage $V_2(s)$ can be represented as

$$V_2(s) = v_{20} + v_{21}s + v_{22}s^2 + v_{23}s^3 + ... \tag{10}$$

These specific forms for the series have been chosen to be consistent with the final value theorem. If an exponential input with amplitude V_{dd} is applied to the aggressor, the response $v_1(t)$ on the aggressor net will converge towards V_{dd} as $t \to \infty$. This is captured by ensuring a nonzero value for v_{10}. Similarly, for the latter equation, $v_2(t)$ approaches 0 as its final value, consistent with the observation that the response on the victim net is limited in time.

Using the series expansions for the voltages V_1 and V_2 and substituting them in Equation (2) leads to:

$$\begin{aligned}(sC_1 + A_{11})(v_{10}s^{-1} + v_{11} + v_{12}s + v_{13}s^2 + ...) - \\ sC_c^T(v_{20} + v_{21}s + v_{22}s^2 + v_{23}s^3 + ...) = B_1(\frac{1}{s} - \frac{1}{s+p}),\end{aligned} \tag{11}$$

$$(sC_2 + A_{22})(v_{20} + v_{21}s + v_{22}s^2 + v_{23}s^3 + ...) -$$
$$sC_c(v_{10}s^{-1} + v_{11} + v_{12}s + v_{13}s^2 + ...) = 0. \quad (12)$$

As in AWE [4], we may conclude that these equations are satisfied if the coefficients of all s^i on the left hand side are the same as those on the right hand side. Hence, we obtain from (11):

$$\begin{aligned}
s^0 &: A_{11}v_{10}p = B_1p, \\
s^1 &: pA_{11}v_{11} + (pC_1 + A_{11})v_{10} = 0, \\
s^2 &: pA_{11}v_{12} + C_1v_{10} + (pC_1 + A_{11})v_{11} - pC_c^Tv_{20} = 0, \\
s^{i\geq 3} &: pA_{11}v_{1i} + C_1v_{1(i-2)} + (pC_1 + A_{11})v_{1(i-1)} - pC_c^Tv_{2(i-2)} - C_c^Tv_{2(i-3)} = 0. \quad (13)
\end{aligned}$$

Solving this for v_{1i} leads to

$$\begin{aligned}
s^0 : \quad v_{10} &= A_{11}^{-1}B_1, \\
s^1 : \quad v_{11} &= -A_{11}^{-1}(pC_1 + A_{11})v_{10}/p, \\
s^2 : \quad v_{12} &= -A_{11}^{-1}(C_1v_{10} + (pC_1 + A_{11})v_{11} - pC_c^Tv_{20})/p, \\
s^{i\geq 3} : \quad v_{1i} &= -A_{11}^{-1}(C_1v_{1(i-2)} + (pC_1 + A_{11})v_{1(i-1)} - pC_c^Tv_{2(i-2)} - C_c^Tv_{2(i-3)})/p. \quad (14)
\end{aligned}$$

Similarly, from (12), the following results can be obtained for v_{2i}:

$$\begin{aligned}
s^0 : \quad v_{20} &= A_{22}^{-1}C_cv_{10}, \\
s^1 : \quad v_{21} &= A_{22}^{-1}(C_cv_{11} - C_2v_{20}), \\
s^{i\geq 2} : \quad v_{2i} &= A_{22}^{-1}(C_cv_{1i} - C_2v_{2(i-1)}). \quad (15)
\end{aligned}$$

In order to obtain a closed form for the voltage $v_2(t)$, let us consider its response to an exponential input (see Figure 1, graph 2). For $t \to 0$, $v_2(t)$ is 0 and for $t \to \infty$, $v_2(t)$ is 0. Using the initial and final value theorems, the following form of voltage function is appropriate:

$$V_2(s) = \frac{a_0 + a_1s + ... + a_{n-2}s^{n-2}}{1 + b_1s + ... + b_{n-1}s^{n-1} + b_ns^n}. \quad (16)$$

In particular, for computational efficiency, we will focus on the approximation of the following form:

$$V_2(s) = \frac{a_0 + a_1s}{1 + b_1s + b_2s^2 + b_3s^3} \quad (17)$$

which has the inverse Laplace transform

$$v_2(t) = c_1 \cdot e^{-\frac{t}{k_1}} + c_2 \cdot e^{-\frac{t}{k_2}} + c_3 \cdot e^{-\frac{t}{k_3}}, \tag{18}$$

where $1/k_1, 1/k_2$ and $1/k_3$ are the poles of the voltage function. In case AWE encounters stability problems, a second order model of the following form is applied:

$$V_2(s) = \frac{a_0}{1 + b_1 s + b_2 s^2} \tag{19}$$

which has the inverse Laplace transform

$$v_2(t) = c_1 \cdot e^{-\frac{t}{k_1}} + c_2 \cdot e^{-\frac{t}{k_2}}, \tag{20}$$

where $1/k_1$ and $1/k_2$ are the poles of the voltage function. It was observed that none of the configurations in our experiments showed an unstable second order model.

Performing moment matching for the expressions for $V_2(s)$ in the equations (12) and (17) leads to:

$$a_0 = v_{20_j} \tag{21}$$

$$a_1 = v_{20_j} b_{1_j} + v_{21_j} \tag{22}$$

and

$$\begin{bmatrix} b_1 \\ b_2 \\ b_3 \end{bmatrix} = \begin{bmatrix} v_{21_j} & v_{20_j} & 0 \\ v_{22_j} & v_{21_j} & v_{20_j} \\ v_{23_j} & v_{22_j} & v_{21_j} \end{bmatrix}^{-1} \begin{bmatrix} -v_{22_j} \\ -v_{23_j} \\ -v_{24_j} \end{bmatrix}. \tag{23}$$

where j is the node number where the noise is computed. In case the approximation of equation (19) is used, similar expressions can be used to find the voltage moments.

5 Incorporating Inductive Effects

We will persist with the notation introduced above, as far as possible and model the input voltage as an exponential function according to (8). $V_1(s)$ and $V_2(s)$ are expanded as described in section 4.

The basic set of equations for a circuit of the type shown in Figure 3, with net 1 being the aggressor and net 2 being the victim net, initially at ground potential, can be written as follows:

$$\begin{bmatrix} C_1 & -C_c^T & 0 & 0 \\ -C_c & C_2 & 0 & 0 \\ 0 & 0 & L_1 & M_{12}^T \\ 0 & 0 & M_{12} & L_2 \end{bmatrix} \begin{bmatrix} \dot{v_1} \\ \dot{v_2} \\ \dot{i_{L_1}} \\ \dot{i_{L_2}} \end{bmatrix} = \begin{bmatrix} -A_{11} & 0 & I_{1L}^T & 0 \\ 0 & -A_{22} & 0 & I_{2L}^T \\ I_{1L} & 0 & 0 & 0 \\ 0 & I_{2L} & 0 & 0 \end{bmatrix} \begin{bmatrix} v_1 \\ v_2 \\ i_{L_1} \\ i_{L_2} \end{bmatrix} + \begin{bmatrix} B_1 \\ 0 \\ 0 \\ 0 \end{bmatrix} v_s, \tag{24}$$

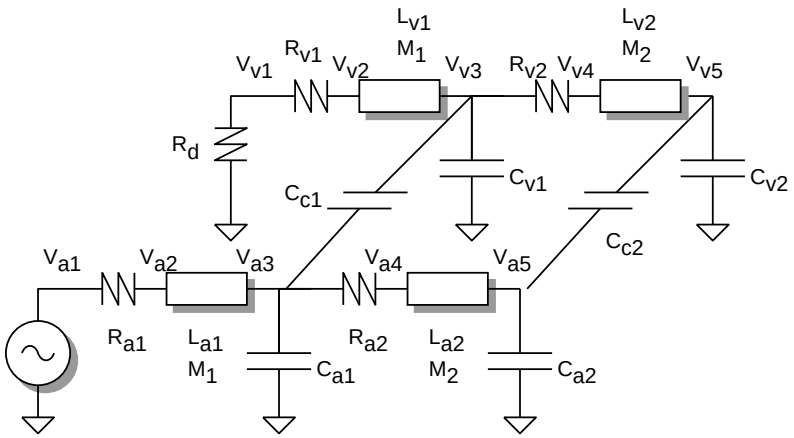

Figure 3. Circuit schematic with aggressor and victim net for coupled noise including inductances. For the sake of simplicity, only two of the n distributed RLC elements have been shown. R_d corresponds to the impedance to ground of the victim net.

where L_1, L_2 and M_{12} corresponds to the self-inductive matrix of aggressor and victim net and the mutual inductance between these wires, respectively. I_{1L} and I_{2L} correspond to matrices consisting of ones and minus ones, representing the voltage difference of the inductors in victim and aggressor nets. This matrix system can be rewritten in the Laplace domain as

$$\begin{aligned} sC_1V_1 - sC_c^TV_2 &= -A_{11}V_1 + B_1V_s, \\ sC_cV_1 - sC_2V_2 &= A_{22}V_2, \\ sL_1i_{L_1} + sM_{12}^Ti_{L_2} &= V_{a,2k} - V_{a,2k+1} \\ sM_{12}i_{L_1} + sL_2i_{L_2} &= V_{v,2k} - V_{v,2k+1}. \end{aligned} \tag{25}$$

Note that the diagonal entries of capacitance matrices C_1 and C_2 correspond to the sum of ground and coupling capacitances, while diagonal entries of the matrix C_c have a positive value and k is an integer variable, resulting in $V_{a,2} - V_{a,3}$, $V_{a,4} - V_{a,5}$, etc.

Hence, the matrices A_{ii}, C_c and C_j from section 4 can be replaced by the matrices X_{ii}, Y_c and Y_j, where X_{ii} represents the matrix including the resistances of the aggressor and victim net as well as the matrices I_{1L} and I_{2L}, while the matrices Y_j and Y_c include the ground capacitances and self inductances from wire j and the coupling capacitances and mutual inductances between aggressor and victim net, respectively.

Similar to the series expansion of the voltages V_1 and V_2, the currents i_{L_1} and i_{L_2} can be

modeled. Hence, the new vectors Z_1 and Z_2 consist of each n voltage nodes and n inductive currents where n represents the number of segments in each of the wires.

For an exponential input, we may expand $i_{L_1}(s)$ and $i_{L_2}(s)$ using the series:

$$i_{L_1}(s) = i_{10} + i_{11}s + i_{12}s^2 + i_{13}s^3 + ... \quad (26)$$

$$i_{L_2}(s) = i_{20} + i_{21}s + i_{22}s^2 + i_{23}s^3 + ... \quad (27)$$

These specific forms for the series have been chosen to be consistent with the final value theorem. If an exponential input with amplitude V_{dd} is applied to the aggressor, the currents i_{L_1} and i_{L_2} have an initial and final value of zero, consistent with the observation that the currents in the victim and aggressor nets are limited in time. Using the series expansions for the voltages Z_1, Z_2 and substituting them in Equation (25) leads to:

$$\begin{aligned}(sY_1 + X_{11})(z_{10}s^{-1} + z_{11} + z_{12}s + z_{13}s^2 + ...) - \\ sY_c^T(z_{20} + z_{21}s + z_{22}s^2 + z_{23}s^3 + ...) = B_1(\frac{1}{s} - \frac{1}{s+p}),\end{aligned} \quad (28)$$

$$\begin{aligned}(sY_2 + X_{22})(z_{20} + z_{21}s + z_{22}s^2 + z_{23}s^3 + ...) - \\ sY_c(z_{10}s^{-1} + z_{11} + z_{12}s + z_{13}s^2 + ...) = 0.\end{aligned} \quad (29)$$

Therefore, the moments z_{1j} and z_{2j} can be computed in the same way as the moments v_{1j} and v_{2j} in section 4.

6 Efficient Computation Techniques

6.1 Circuit Interpretation and Computation

As in Devgan's work, we may ascribe a physical meaning to these equations. For the computation of the coefficients a_{i_j} and b_{i_j} of the Laplace transform, entirely six moments of V_1 and V_2 are required. For the sake of simplicity, we always refer to the moments z_{ij} instead of v_{ij} for purely capacitive coupled and z_{ij} for capacitive and inductive coupled nets. For the computation of v_{ij}, the inductance parts have to be neglected.

- The zeroth moment z_{10} always corresponds to the voltage V_{dd} at each node. On the other hand, z_{20}, which are the counterparts of the noise metric computed by Devgan (except that

we use an exponential instead of an infinite ramp), may be computed by replacing each coupling capacitor by a current source of value $C_c V_{dd}$ and calculating the voltages in the resulting network, while the self inductances are shorted.

- Finding z_{11} involves the solution of the aggressor net with all coupling capacitances removed, and all self-capacitances to ground, C_{1_j}, replaced by a current source of value $-C_{1_j} z_{10_j}$ and each node has an initial voltage of z_{10_j}/p. All self- and mutual inductances have to be additionally replaced by voltage sources of value $L_{1_j} z_{10_j}$ and $M_{12_j} z_{10_j}$. The solution to the resulting circuit yields the vector z_{11}.

- Finding z_{21} involves the solution of the victim net with all coupling capacitances replaced by current sources of value $C_{1_j} z_{11_j}$,all self-capacitances to ground, C_{2_j}, replaced by a current source of value $-C_{2_j} z_{20_j}$, all mutual inductances M_{12_j} replaced by voltage sources of value $M_{12_j} z_{11_j}$ and all self inductances replaced by voltage sources of value $L_{2_j} z_{20_j}$. The solution to the resulting circuit yields the vector z_{21}. All higher moments z_{2i}, $i > 1$ are similarly computed by choosing the corresponding current sources as $C_{1_j} z_{1i_j}$ and $-C_{2_j} z_{2(i-1)_j}$ as well as the corresponding voltage sources as $M_{12_j} z_{2(i-1)_j}$ and $L_{2_j} z_{2(i-1)_j}$.

- Finding z_{12} involves the solution of the aggressor net with all coupling capacitances replaced by current sources of value $C_{c_j} z_{20_j}$, and all self-capacitances to ground, C_{1_j}, replaced by a current source of value $-C_{1_j}(z_{11} + z_{10_j}/p)$ and each node has an initial voltage of z_{11_j}/p. The self- and mutual inductances L_{1_j}, M_{12_j} have to be replaced by voltage sources of value $L_{1_j}(z_{11} + z_{10_j}/p)$ and $M_{12_j}(z_{11} + z_{10_j}/p)$. The solution to the resulting circuit yields the vector z_{12}.

- All higher moments $z_{1i}, i > 2$ can be computed by replacing the coupling capacitances C_{c_j} by current sources of value $C_{c_j}(z_{2(i-2)_j} + z_{2(i-3)_j}/p)$, and all ground capacitances C_{1_j} replaced by current sources of value $-C_{1_j}(z_{1(i-2)_j}/p + z_{1(i-1)})$ while all nodes j have an initial voltage of $z_{1(i-1)_j}/p$. The self- and mutual inductances L_{2_j}, M_{12_j} have to be replaced by voltage sources of value $L_{2_j}(z_{1(i-2)_j}/p + z_{1(i-1)})$ and $M_{12_j}(z_{1(i-2)_j}/p + z_{1(i-1)})$.

Once all required moments are computed, the poles and residues of the victim net can be obtained. The order in which the moments are calculated is $z_{20}, z_{11}, z_{21}, z_{12}, z_{22}, z_{13}, \cdots$.

6.2 Computational Complexity

The computational complexity of the proposed metric can be obtained by examining the equations (14) to (20). To obtain v_{20}, two tree traversals and one multiplication of a diagonal matrix vector by a vector are required. The tree traversal and the multiplication are of the order $O(n)$, where n is the number of segment points (see section 6). In order to obtain v_{11}, two tree traversals and a diagonal matrix-vector multiplication are required. All higher moments $v_{2(i-1)}$ and v_{1i} simply require two additional tree traversals per moment and two diagonal matrix by vector multiplications. All these operations are of the order of $O(n)$. The complexity for the computation of necessary moments for the voltage function in Equation (17) corresponds to 20 tree traversals and 18 diagonal matrix by vector multiplications. After the computation of all necessary moments the residues and poles of the voltage function have to be computed. This requires the solution of a 3×3 system and can be solved in $O(1)$ for each node resulting in the coefficients a_i and b_i. Finding the roots of a third order function can be performed in linear time for n nodes and is of the order of $O(n)$.

Compared with the metric of Devgan, this corresponds to an increase in the number of tree traversals and multiplication/division by 6x and 20x, respectively. However, by realizing that Devgan's scheme required less than half a second to compute the noise in a circuit with 500,000 elements, this increase in complexity is tolerable.

7 Results and Comparison

In accordance with [2], SPICE-files have been obtained for five different wire lengths, varying from 1mm to 5mm for the aggressor net and victim net, respectively. The wire resistances and capacitances have been distributed every $100\mu m$. Hence, the number of segment points is equal to the length of the victim net divided by $100\mu m$. The driver of the aggressor net is simulated as a voltage source with a time constant that is calculated based on the effective capacitance, C_{eff} [18]. At the end of the wires, a load capacitance of 50fF is placed to model a possible fan-out.

Table 3. Noise simulation results in mV of HSPICE , using a 0.18μm CMOS technology and V_{dd}=1.8V. The wires have been spaced at twice the minimum distance leading to a resistance, a ground and coupling capacitance per mm of 250 Ω, 51.4 fF and 58.3 fF, respectively.

	Victim impedance: 200 Ω					
wire length, agg-vic	0.05ns	0.1ns	0.25ns	0.5ns	0.75ns	1.0ns
1-1mm	296	233	145	92	67	54
1-2mm	213	177	120	80	60	48
1-3mm	152	133	96	67	52	43
1-4mm	112	101	77	56	45	37
1-5mm	84	77	63	47	38	33
2-1mm	261	206	133	85	64	51
2-2mm	393	352	264	190	150	124
2-3mm	312	288	227	170	136	114
2-4mm	247	234	193	148	122	104
2-5mm	197	190	163	130	107	93
3-1mm	255	198	125	81	61	48
3-2mm	350	315	242	177	142	118
3-3mm	423	403	341	268	224	192
3-4mm	355	344	301	244	205	178
3-5mm	298	293	262	218	187	164
4-1mm	254	197	123	78	58	47
4-2mm	334	297	226	166	133	112
4-3mm	383	366	314	252	211	183
4-4mm	433	425	386	326	283	251
4-5mm	378	373	345	298	262	234
5-1mm	254	197	123	78	58	46
5-2mm	331	292	220	160	127	107
5-3mm	362	344	294	236	200	173
5-4mm	398	392	358	306	267	238
5-5mm	438	435	412	366	328	297

Table 4. Noise simulation results in mV of the proposed metric, using a 0.18μm CMOS technology and V_{dd}=1.8V. The wires have been spaced at twice the minimum distance leading to a resistance, a ground and coupling capacitance per mm of 250 Ω, 51.4 fF and 58.3 fF, respectively.

	Victim impedance: 200 Ω					
wire length, agg-vic	0.05ns	0.1ns	0.25ns	0.5ns	0.75ns	1.0ns
1-1mm	297	233	145	92	67	54
1-2mm	211	176	120	80	60	48
1-3mm	150	131	95	67	52	43
1-4mm	108	98	76	56	45	37
1-5mm	82	76	62	47	38	33
2-1mm	258	207	133	86	64	51
2-2mm	391	352	265	191	150	124
2-3mm	310	286	227	170	136	114
2-4mm	244	231	191	148	122	103
2-5mm	195	186	160	128	107	93
3-1mm	235	195	123	80	60	48
3-2mm	336	314	243	178	142	118
3-3mm	417	402	341	270	224	193
3-4mm	352	342	300	243	205	178
3-5mm	297	290	260	217	186	163
4-1mm	226	180	122	75	57	46
4-2mm	312	287	226	167	134	113
4-3mm	370	361	315	253	212	183
4-4mm	426	421	385	326	283	251
4-5mm	374	371	344	297	262	234
5-1mm	225	177	115	74	56	45
5-2mm	298	274	220	157	126	106
5-3mm	338	328	294	237	201	174
5-4mm	387	380	357	307	268	238
5-5mm	430	430	410	366	328	297

Table 5. The relative error in percent between the proposed metric and the HSPICE simulations, using a 0.18μm CMOS technology and V_{dd}=1.8V. The wires have been spaced at twice the minimum distance leading to a resistance, a ground and coupling capacitance per mm of 250 Ω, 51.4 fF and 58.3 fF, respectively.

	Victim impedance: 200 Ω					
wire length, agg-vic	0.05ns	0.1ns	0.25ns	0.5ns	0.75ns	1.0ns
1-1mm	0.4	0.2	0.2	0.1	0	0
1-2mm	-0.8	-0.6	-0.3	-0.1	-0.1	0
1-3mm	-1.8	-1.5	-0.7	-0.3	-0.2	-0.1
1-4mm	-2.6	-2.3	-1.2	-0.5	-0.3	-0.2
1-5mm	-3	-2.8	-1.6	-0.7	-0.4	-0.3
2-1mm	-1	0.5	0.5	0.4	0.3	0.3
2-2mm	-0.4	0.1	0.2	0.1	0.1	0.1
2-3mm	-0.7	-0.5	-0.3	-0.2	-0.1	-0.1
2-4mm	-1.2	-1.3	-0.8	-0.5	-0.4	-0.3
2-5mm	-1.4	-2	-1.5	-1	-0.6	-0.5
3-1mm	-8.6	-1.8	-2.3	-1.7	-1.2	-0.7
3-2mm	-4.1	-0.1	0.6	0.5	0.4	0.3
3-3mm	-1.4	-0.4	0.1	0.2	0.1	0.1
3-4mm	-0.8	-0.7	-0.3	-0.1	-0.1	0
3-5mm	-0.7	-1.1	-0.8	-0.5	-0.4	-0.3
4-1mm	-12.2	-10	-1.6	-4.2	-2.5	-1.5
4-2mm	-7.1	-3.7	0.3	0.5	0.4	0.4
4-3mm	-3.7	-1.7	0.3	0.4	0.4	0.4
4-4mm	-1.6	-1	-0.1	0.1	0.1	0.1
4-5mm	-1	-0.8	-0.4	-0.2	-0.1	-0.1
5-1mm	-12.6	-11	-7.4	-5.3	-3.6	-2.6
5-2mm	-10.7	-7	0.2	-1.8	-1.6	-1.3
5-3mm	-7.1	-5.2	0	0.5	0.6	0.5
5-4mm	-3.1	-3.2	-0.1	0.3	0.3	0.3
5-5mm	-2.2	-1.4	-0.4	0	0.1	0.1

Table 6. Noise simulation results in mV of HSPICE , using a 0.18μm CMOS technology and V_{dd}=1.8V. The wires have been spaced at twice the minimum distance leading to a resistance, a ground and coupling capacitance per mm of 250 Ω, 51.4 fF and 58.3 fF, respectively.

	Victim impedance: 1000 Ω					
wire length, agg-vic	0.05ns	0.1ns	0.25ns	0.5ns	0.75ns	1.0ns
1-1mm	455	387	274	190	147	122
1-2mm	333	295	221	161	128	107
1-3mm	248	227	180	136	111	94
1-4mm	190	178	147	116	96	83
1-5mm	148	143	123	100	84	74
2-1mm	410	357	261	185	145	120
2-2mm	530	495	403	311	255	218
2-3mm	430	410	345	273	228	197
2-4mm	350	338	294	240	204	178
2-5mm	287	281	252	211	182	161
3-1mm	393	340	248	177	140	116
3-2mm	481	454	378	297	247	212
3-3mm	542	527	467	388	333	293
3-4mm	463	454	412	350	304	270
3-5mm	396	391	362	313	275	247
4-1mm	391	335	242	172	136	113
4-2mm	455	427	357	284	237	205
4-3mm	498	487	438	370	321	284
4-4mm	540	534	498	437	388	351
4-5mm	476	472	447	398	357	325
5-1mm	391	334	240	170	134	111
5-2mm	447	417	345	273	228	197
5-3mm	470	460	414	352	307	273
5-4mm	503	498	470	416	373	337
5-5mm	535	532	512	467	426	393

Table 7. Noise simulation results in mV of the proposed metric, using a 0.18μm CMOS technology and V_{dd}=1.8V. The wires have been spaced at twice the minimum distance leading to a resistance, a ground and coupling capacitance per mm of 250 Ω, 51.4 fF and 58.3 fF, respectively.

	Victim impedance: 1000 Ω					
wire length, agg-vic	0.05ns	0.1ns	0.25ns	0.5ns	0.75ns	1.0ns
1-1mm	456	388	274	190	147	122
1-2mm	331	294	221	161	127	107
1-3mm	245	226	180	136	111	94
1-4mm	187	176	146	115	96	83
1-5mm	146	141	122	98	84	73
2-1mm	404	360	262	185	145	120
2-2mm	526	496	404	311	255	218
2-3mm	427	407	344	273	228	197
2-4mm	348	335	293	240	203	177
2-5mm	286	278	248	208	181	160
3-1mm	371	333	250	178	141	116
3-2mm	468	452	381	298	248	213
3-3mm	532	523	468	390	334	294
3-4mm	458	451	411	350	304	270
3-5mm	394	388	360	312	275	246
4-1mm	371	327	242	173	136	113
4-2mm	432	412	360	285	238	206
4-3mm	486	476	440	372	322	285
4-4mm	530	525	498	438	390	351
4-5mm	471	467	446	398	358	325
5-1mm	363	313	234	168	132	110
5-2mm	417	385	340	274	230	198
5-3mm	452	440	413	354	308	274
5-4mm	491	486	467	417	374	338
5-5mm	525	521	508	467	427	393

Table 8. The relative error between the proposed metric and the HSPICE simulations, using a 0.18μm CMOS technology and V_{dd}=1.8V. The wires have been spaced at twice the minimum distance leading to a resistance, a ground and coupling capacitance per mm of 250 Ω, 51.4 fF and 58.3 fF, respectively.

	Victim impedance: 1000 Ω					
wire length, agg-vic	0.05ns	0.1ns	0.25ns	0.5ns	0.75ns	1.0ns
1-1mm	0.3	0.2	0.1	0	0	0
1-2mm	-0.4	-0.3	-0.1	-0.1	-0.1	0
1-3mm	-1.1	-1	-0.4	-0.2	-0.1	-0.1
1-4mm	-1.5	-1.5	-0.7	-0.3	-0.2	-0.1
1-5mm	-1.6	-1.7	-1.1	-0.5	-0.3	-0.2
2-1mm	-1.5	0.6	0.5	0.3	0.2	0.1
2-2mm	-0.7	0.2	0.3	0.2	0.1	0.1
2-3mm	-0.4	-0.3	-0.1	0	0	0
2-4mm	-0.5	-0.8	-0.6	-0.3	-0.2	-0.2
2-5mm	-0.7	-1.2	-1.1	-0.6	-0.4	-0.3
3-1mm	-6.3	-2.2	0.4	0.5	0.4	0.4
3-2mm	-2.7	-0.6	0.6	0.5	0.4	0.3
3-3mm	-2.1	-0.7	0.2	0.3	0.2	0.2
3-4mm	-1	-0.6	-0.1	0	0	0.1
3-5mm	-0.4	-0.6	-0.6	-0.3	-0.2	-0.2
4-1mm	-5.8	-2.4	0	0.2	0.2	0.3
4-2mm	-5.4	-4.2	0.5	0.6	0.6	0.5
4-3mm	-2.7	-2.5	0.3	0.5	0.4	0.4
4-4mm	-2	-1.7	-0.1	0.2	0.3	0.2
4-5mm	-1.3	-1.1	-0.3	0	0	0.1
5-1mm	-7.8	-7	-2.7	-1.2	-1.5	-1.5
5-2mm	-7.4	-8.4	-1.7	0.5	0.6	0.5
5-3mm	-4.3	-4.5	-0.5	0.6	0.6	0.6
5-4mm	-2.6	-2.7	-0.4	0.4	0.4	0.4
5-5mm	-2	-2.4	-0.6	0.1	0.2	0.2

The simulations have been performed for victim impedances of 200 Ω and 1000 Ω, respectively.

The results of the HSPICE simulations are presented in the Tables 3 and 6 for a 180nm CMOS technologies. Aggressors and victims of various length are chosen. The entry 5mm-1mm implies an aggressor net of length 5mm and a victim net that is 1mm long. The noise is always measured at the end of the victim net. The values 0.05ns. 0.1ns, 0.25ns, 0.5ns, 0.75ns and 1ns correspond to the time constant of the input source.

Tables 3 and 6 show the results of the HSPICE simulations, while Tables 4 and 7 indicate the results obtained by the proposed metric. Finally, Tables 5 and 8 present the relative error introduced by the proposed metric. It can be seen that the results of the new metric have a very good accuracy compared to SPICE. The noise is slightly under-estimated for some victim nets due to instability problems of the third order model and resulting use of a second order model. The error in the noise prediction is caused by the computation of AWE moments and the corresponding reduction of a n^{th}-order Laplace transform to a third order model. By comparing the results of the new metric with the results of Devgan (these results are shown in Section 3.1), the improvement in noise estimation is obvious. While the noise is over-estimated by up to two orders of magnitude using Devgan's metric, the proposed metric provides results that are close to the actual SPICE simulations. Our experimental results suggest that this metric underestimates the noise in many cases, but never by more than about 10%. This is a very acceptable level of accuracy as compared to other sources of error such as inaccuracies in extracting and modeling the resistances and capacitances for the line.

8 Conclusion

This paper presented a new method for coupled noise estimation. The proposed metric computes the noise according to the sink capacitances and conductances of the aggressor net and the victim net, respectively, the coupling capacitance between those two nets and the time constant of the aggressor signal. The noise waveform is computed using a closed form leading to a short computation time. While previously the coupling noise was over-estimated by up to two orders of magnitude, assuming slew rates of less than 100ps and long or medium length wires, the coupling noise can be computed within an accuracy of 11.4% compared to SPICE. This results have been

obtained by comparing the proposed metric results with SPICE simulation results.

References

[1] J. Cong, "Challenges and opportunities for design innovations in nanometer technologies," tech. rep., Semiconductor Research Corporation, 1998.

[2] Semiconductor Industry Association, "National technology roadmap for semiconductors," 1997.

[3] L. W. Nagel, "SPICE2, A computer program to simulate semiconductor circuits," in *Technical Report ERL-M520*, (UC-Berkeley), May 1975.

[4] L. T. Pillage and R. A. Rohrer, "Asymptotic waveform evaluation for timing analysis," *IEEE Transactions on Computer-Aided Design*, vol. 9, pp. 352–366, Apr. 1990.

[5] P. Feldmann and R. W. Freund, "Efficient linear circuit analysis by Padé approximation via the Lanczos process," *IEEE Transactions on Computer-Aided Design*, vol. 14, pp. 639–649, May 1995.

[6] A. Odabasioglu, M. Celik, and L. T. Pileggi, "PRIMA: Passive reduced-order interconnect macromodeling algorithm," *IEEE Transactions on Computer-Aided Design*, vol. 17, pp. 645–654, Aug. 1998.

[7] K. Shepard and V. Narayanan, "Noise in submicron digital design," in *Proceedings of IEEE/ACM International Conference on Computer Aided Design*, pp. 524–531, 1996.

[8] K. Shepard, V. Narayanan, P. C. Elmendorf, and G. Zheng, "GlobalHarmony: Coupled noise analysis for full-chip RC interconnect networks," in *Proceedings of the IEEE/ACM International Conference on Computer-Aided Design*, pp. 139–146, 1997.

[9] A. Devgan, "Efficient coupled noise estimation for on-chip interconnects," in *Proceedings of the IEEE/ACM International Conference on Computer-Aided Design*, pp. 147–151, 1997.

[10] C. J. Alpert, A. Devgan, and S. T. Quay, "Buffer insertion for noise and delay optimization," in *Proceedings of the ACM/IEEE Design Automation Conference*, pp. 362–367, 1998.

[11] P. Morton and W. Dai, "An efficient sequential quadratic programming formulation of optimal wire spacing for crosstalk noise avoidance routing," in *ACM International Symposium on Physical Design*, pp. 22–28, 1999.

[12] T. Gao and C. L. Liu, "Minimum crosstalk switchbox routing," in *Proceedings of the IEEE/ACM International Conference on Computer-Aided Design*, pp. 610–615, 1994.

[13] T. Xue, E. S. Kuh, and D. Wang, "Post global routing crosstalk risk estimation and reduction," in *Proceedings of the IEEE/ACM International Conference on Computer-Aided Design*, pp. 302–309, 1996.

[14] H. Zhou and D. F. Wong, "Global routing with crosstalk constraints," in *Proceedings of the ACM/IEEE Design Automation Conference*, pp. 374–377, 1998.

[15] M. Kuhlmann, S. S. Sapatnekar, and K. K. Parhi, "Efficient crosstalk estimation," in *Proc. of IEEE 1999 International Conf. on Computer and Design*, pp. 266–272, Oct. 1999.

[16] C. L. Phillips, *Signals, systems and transforms*, ch. 7. Upper Saddle River, N.J.: Prentice Hall, 2nd ed., 1999.

[17] J. Rubinstein, P. Penfield, and M. A. Horowitz, "Signal delay in RC tree networks," *IEEE Transactions on Computer-Aided Design*, vol. CAD-2, pp. 202–211, Jul. 1983.

[18] J. Qian, S. Pullela, and L. T. Pillage, "Modeling the effective capacitance of RC interconnect of CMOS gates," *IEEE Transactions on Computer-Aided Design*, vol. 13, pp. 1526–1535, Dec. 1994.